ward curving of the slab (Fig. 2). On the other hand, the double-planed seismicity in northern Chile is observed beneath the volcanic Andean belt, suggesting it is associated with the generation of magma and the production of arc volcanoes. Thus, it could be explained as a result of a phase change in the slab, as was recently suggested for the Tonga subduction zone (*22*).

Kirby and Hacker (*23, 24*) modeled the distribution of stresses induced by changes in pressure and temperature in the subducting lithosphere at depths of between 90 to 150 km. They argued that oceanic plates have a laminated structure with a thin crust on the top composed of basaltic minerals, overlying a thicker mantle composed mainly of peridotite. According to their numerical results (*25*), the subducting basaltic crust transforms into the denser eclogite as a result of the increased pressure induced during the plate descent and the dehydration of the oceanic crust at the source of the volcanic arc. However, the peridotite composing the upper mantle does not suffer a phase change because it is stable to greater pressure.

This differential volume change produces tensional deformation in the transformed crustal layer and induces a smaller compressional deformation near the top of the underlying mantle (*23, 24*). The distribution of stresses induced by this phase change would explain the inverted double seismic zone observed in northern Chile and the fact that it is observed mainly with events of smaller magnitude. Furthermore, the separation between the stress sheets suggested by the numerical results is similar to that observed in both Iquique and Antofagasta (~15 km).

REFERENCES AND NOTES

1. B. Isacks and P. Molnar, *Nature* **223**, 1121 (1969).
2. ______, *Rev. Geophys.* **9**, 103 (1971).
3. D. Forsyth and S. Uyeda, *Geophys. J. R. Astron. Soc.* **43**, 163 (1975).
4. N. Vlaar and M. Wortel, *Tectonophysics* **32**, 331 (1976).
5. M. Vassiliou, B. Hager, A. Raefsky, *J. Geodyn.* **1**, 11 (1984).
6. W. Spence, *Rev. Geophys.* **25**, 55 (1987).
7. Double seismic zones have been reported beneath Tohoku, Japan, by N. Umino and A. Hasegawa [*Seismol. Soc. Jpn. J.* **28**, 125 (1975)], A. Hasegawa *et al.* [*Tectonophysics* **47**, 43 (1978)], and T. Yoshii [*ibid.* **55**, 349 (1979)]; in the Tohoku-Hokkaido region, Japan, by N. Umino *et al.* [*Seismol. Soc. Jpn. J.* **37**, 523 (1984)]; in Hokkaido, Japan, by S. Suzuki *et al.* [*Tectonophysics* **96**, 59 (1983)]; in Kurile-Kamchatka by W. Stauder and L. Mualchin [*J. Geophys. Res.* **81**, 297 (1976)]; and in the eastern Aleutians by M. Reyners and K. Coles [*ibid.* **87**, 356 (1982)] and L. House and K. Jacob [*ibid.* **88**, 9347 (1983)]. H. Kawakatsu (*11*) gives a thorough review of these and other regions where double seismic zones have been identified.
8. K. Fujita and H. Kanamori, *Geophys. J. R. Astron. Soc.* **66**, 131 (1981).
9. E. R. Engdahl and C. H. Scholtz, *Geophys. Res. Lett.* **4**, 473 (1977).
10. B. Isacks and M. Barazangi, in *Island Arcs, Deep-Sea Trenches, and Back-Arc Basins*, M. Talwani and W. Pitman III, Eds. (Maurice Ewing Ser. 1, American Geophysical Union, Washington, DC, 1977), pp. 99–114.
11. H. Kawakatsu, *J. Geophys. Res.* **91**, 4811 (1986).
12. Proposed mechanisms to explain double seismic zones include stresses associated with phase changes [K. Veith, thesis, Southern Methodist University (1974)], elastic unbending of the slabs (*9, 11*), sagging of the subducted slab under its own weight [T. Yoshii, *Kagaku* **47**, 170 (1977), N. H. Sleep, *J. Geophys. Res.* **84**, 4565 (1979)], and thermo-elastic stresses [K. Goto *et al.*, *Tectonophysics* **112**, 111 (1985); L. S. House and K. H. Jacob, *Nature* **295**, 587 (1982)]. Also, Spence (*6*) suggested that the tensional earthquakes reflect slab pull forces, whereas the shallower compressional earthquakes reflect local resistance to rapid down-dip plate motion.
13. C. DeMets, R. G. Argus, S. Stein, *Geophys. J. Int.* **101**, 425 (1990).
14. D. Comte and M. Pardo, *Nat. Hazards* **4**, 23 (1991).
15. D. Comte *et al.*, *Geophys. J. Int.*, in press.
16. D. Comte, S. Roecker, G. Suárez, *ibid.*, in press.
17. L. Rivera and A. Cisternas, *Bull. Seismol. Soc. Am.* **80**, 600 (1990).
18. L. Astiz, T. Lay, H. Kanamori, *Phys. Earth Planet. Inter.* **53**, 80 (1988).
19. M. Araujo and G. Suárez, *Geophys. J. Int.*, in press.
20. D. Comte and G. Suárez, in preparation.
21. M. Kono, Y. Takahasho, Y. Fukao, *Tectonophysics* **112**, 211 (1985).
22. D. Wiens, J. McGuire, P. Shore, *Nature* **364**, 790 (1993).
23. S. Kirby and B. Hacker, *Eos* **76**, 70 (1993).
24. ______, *ibid.* **72**, 481 (1991).
25. R. Delinger and S. Kirby, *ibid.*, p. 481.

26. We thank C. Mendoza, W. Spence, and two anonymous reviewers for comments that greatly improved this paper. Institut Français de Recherche Scientifique pour le Développement en Coopération (ORSTOM), France, and the International Development Research Centre (IDRC), Canada, offered financial support to conduct the microearthquake investigations. This work was partially funded by Fundación Andes, Chile, grant C-52040. This work was completed while G.S. was visiting the U.S. Geological Survey in Golden, CO.

27 July 1993; accepted 29 October 1993

Modes of Tilting During Extensional Core Complex Development

Drew S. Coleman and J. Douglas Walker

Crustal extension and formation of the Mineral Mountains core complex, Utah, involved tilting of the Mineral Mountains batholith and associated faults during hanging wall and footwall deformation. The batholith was folded in the hanging wall of the Beaver Valley fault between 11 and 9 million years ago yielding about 45° of tilt. Subsequently, the batholith was unroofed along the Cave Canyon detachment fault, and the batholith and fault were tilted approximately 40° during footwall uplift. Recognition of deformed dikes beneath the detachment fault establishes the importance of footwall tilt during formation of extensional core complexes and demonstrates that footwall rebound can be an important process during extension.

Extensional deformation thins the continental crust and results in uplift, cooling, and exposure of ductilely deformed deeper crustal rocks at the Earth's surface in regions known as metamorphic core complexes (*1*). Various models for the development of core complexes and ductile low-angle faults associated with them have been proposed. Models in which extension occurs on an initially steeply or moderately dipping fault that is tilted to low angles through subvertical simple-shear or flexural rotation of the footwall require some tilting to be synchronous with uplift and cooling (*2*). If extension occurs on a low-angle fault, no tilt associated with cooling is predicted (*3, 4*). Many core complexes are comprised dominantly of young batholiths, leading some workers to suggest that cooling and ductile deformation are directly related to intrusion of magmas (*4*). Because batholiths are readily datable, the timing of intrusion, cooling, and faulting can be well established. However, batholiths generally lack planar markers used to determine the structure of core complexes, and thus evaluation of tilting can be difficult. In this report we present data for a dike swarm in the Mineral Mountains batholith that establish the absolute timing of intrusion and deformation in the region and allow estimation of tilting during extension.

The Mineral Mountains (Fig. 1) lie along the southern projection of the Sevier Desert detachment fault (*5, 6*) and are composed dominantly of the 25- to 17-million-year-old granitic Mineral Mountains batholith (*7–14*). The batholith and its wall rocks make up an extensional core complex (*15*), lying in the footwall of the Cave Canyon detachment fault (*10, 12, 16*) and the hanging wall of the listric Beaver Valley fault (*5, 7*). However, the relative timing of motion on these faults has not been clear. Price and Bartley (*15*) suggested that the Cave Canyon detachment fault was initially moderately dipping

D. S. Coleman, Massachusetts Institute of Technology, Department of Earth Atmospheric and Planetary Sciences, 54-1126, Cambridge, MA 02139.
J. D. Walker, Department of Geology, 120 Lindley Hall, University of Kansas, Lawrence, KS 66044.

(30°) and was subsequently tilted to horizontal during footwall uplift. This model predicts that the batholith and its wall rocks should also be tilted.

The northern end of the Mineral Mountains batholith intrudes flat-lying Cambrian rocks and the shallowly dipping Antelope Mountain thrust fault, which is overlain by horizontal Tertiary conglomerates (Fig. 1) (8, 17). Wall rocks on the eastern side include steeply dipping Oligocene volcanic rocks and Paleozoic rocks cut by a now vertically dipping thrust fault (Fig. 1) (7, 9–11, 18). In this same area, the Oligocene volcanic rocks are angularly overlain by moderately dipping Gillies Hill rhyolite flows that erupted 9 million years ago (Ma) (19).

The northern and eastern sides of the Mineral Mountains are intruded by a swarm of rhyolite porphyry and diabase dikes that are the youngest phase of the batholith (Fig. 1) (10–12). On the north end of the batholith, at Antelope Mountain, dikes dip steeply, strike to the north, and intrude shallowly dipping Cambrian strata. In contrast, on the east side of the batholith, the dikes are nearly horizontal and intrude steeply dipping Paleozoic strata (10, 11).

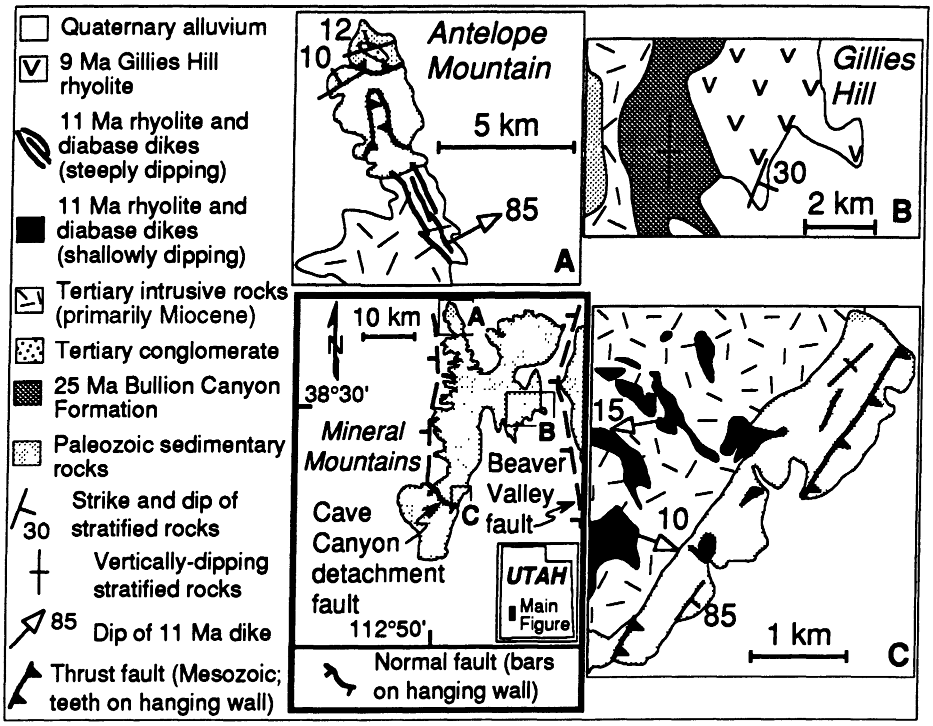

Fig. 1. Simplified geology of the Mineral Mountains. Central figure shows the general location of the range and locations of insets. (**A**) Simplified geology of the Antelope Mountain area (7, 8). Orientations of the thrust faults and the Cambrian rocks are complicated by Tertiary extension but are essentially flat-lying. Attitude shown for Tertiary rocks is the dip of the basal unconformity derived from map pattern. Rhyolite and diabase dikes are steeply dipping. (**B**) Simplified geology of the Gillies Hill area (9). Note that 25-million-year-old Bullion Canyon Formation dips steeply whereas the 9-million-year-old Gillies Hill rhyolite dips moderately. (**C**) Simplified geology of the southeast corner of the Mineral Mountains batholith (9, 10). Orientation of Paleozoic rocks is complicated by folding associated with thrust faulting, but is generally steeply dipping to overturned. Rhyolite and diabase dikes are essentially horizontal in this area.

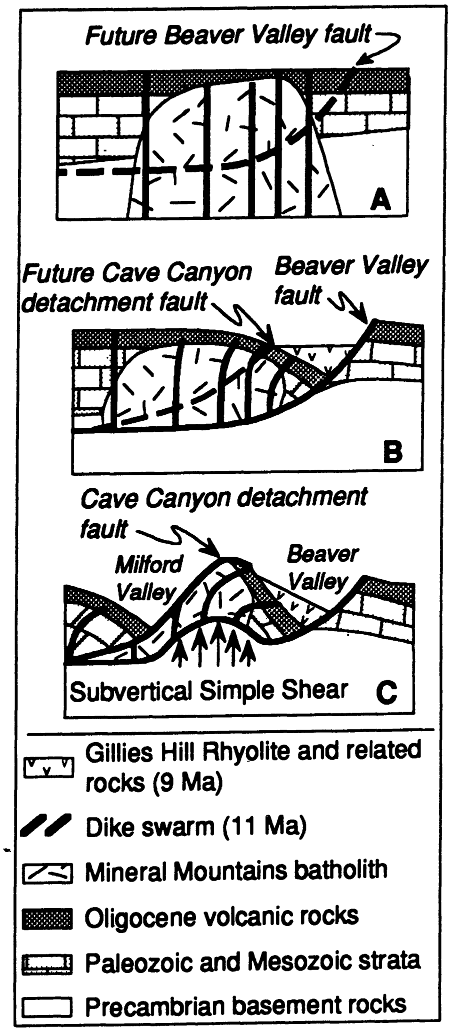

Fig. 3. Schematic east-west cross sections across the Mineral Mountains showing the development of the core complex. Vertical scale about 10 km, with slight vertical exaggeration. Effects of erosion are not shown. (**A**) Intrusion of rhyolite-diabase dike swarm at 11 Ma into the batholith and flat-lying stratified wall rocks. (**B**) Motion along the listric Beaver Valley fault between 11 and 9 Ma causes up to 45° of eastward tilt in a roll-over anticline. Rocks below the Beaver Valley fault are not detailed in this or the next frame. (**C**) Motion along the Cave Canyon detachment causes unroofing of the core complex with uplift accomplished by subvertical simple shear. Gillies Hill rhyolite is tilted to 30° dips and the Cave Canyon detachment fault is folded over the top of the range.

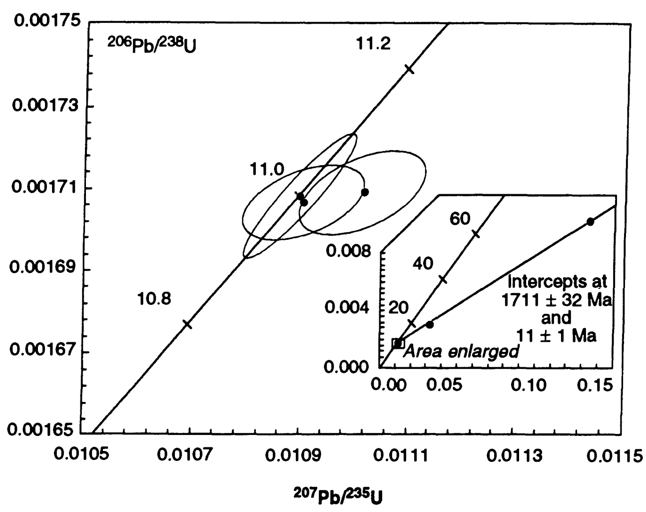

Fig. 2. Concordia plot for zircons from rhyolite porphyry dike (MM88-19) (21). The best estimate of the age of the dike is 11.0 Ma, the $^{238}U/^{206}Pb$ ages of the three most concordant points. The inheritance age agrees extremely well with published ages (1720 Ma) for basement rocks on the western side of the range (13).

Table 1. Uranium-lead isotopic data for zircons in rhyolite porphyry dike (MM88-19). Zircon fractions are designated as magnetic (m) and nonmagnetic (nm) in terms of degrees tilt on a Frantz LB-1 magnetic separator. The a indicates population of acicular grains and e indicates population of equant grains. Number in parentheses is the number of grains analyzed. Sample weights are estimated using a video monitor with a gridded screen and are known to within 10%. Com, total common Pb.

Fractions	Weight (mg)	Concentrations		Atomic ratios								Ages (Ma)			Com Pb (pg)
		U (ppm)	Pb* (ppm)	$^{206}Pb/^{204}Pb$†	$^{208}Pb/^{206}Pb$*	$^{206}Pb/^{238}U$‡	% err	$^{207}Pb/^{235}U$‡	% err	$^{207}Pb/^{206}Pb$‡	% err	$^{206}Pb/^{238}U$	$^{207}Pb/^{235}U$	$^{207}Pb/^{206}Pb$	
m1#2a (65)	0.03	1027	2.1	1907	0.314	0.00171	0.99	0.0109	1.1	0.04626	0.37	11.0	11.0	11.2	5.2
m3a (102)	0.08	720.3	1.5	258.1	0.352	0.00171	0.54	0.0109	1.1	0.04634	0.91	11.0	11.0	15.3	27
m2a (115)	0.07	666.4	1.4	225.9	0.345	0.00171	0.61	0.0110	1.1	0.04675	0.91	11.0	11.1	36.5	27
nm1e (49)	0.06	816.6	2.7	384.7	0.211	0.00297	0.38	0.0285	0.58	0.06947	0.43	19.1	28.5	913	27
m1#1e (92)	0.05	2052	21	24730	0.089	0.00997	0.09	0.1307	0.17	0.09511	0.15	63.9	125	1530	5.9

*Radiogenic Pb. †Measured ratio corrected for fractionation only; Pb fractionation correction is 0.1% ± 0.03% per atomic mass unit. ‡Corrected for fractionation, spike, blank, and initial common Pb; U blank = 1 pg ± 50%; Pb blank = 3.5 pg ± 50%. Initial common Pb composition is the average of two analyses of other rhyolite porphyry dikes from the batholith (*14*): $^{206}Pb/^{204}Pb$ = 17.9, $^{207}Pb/^{204}Pb$ = 15.5, $^{208}Pb/^{204}Pb$ = 37.8. Errors are reported in percent at the 2 sigma confidence interval.

Sparse dikes of this swarm on the west side of the batholith are vertical (*11*).

Thus, the orientations of Mesozoic thrust faults, Paleozoic strata, and dikes change 90° across the batholith, but no faults have been identified between these areas (*7, 10–12*). Taken alone, wall rock orientation could be explained by deformation related to intrusion of the batholith, and the orientation of the dikes could be interpreted to be the result of differences in original intrusive orientation. However, the Tertiary conglomerate at Antelope Mountain and the Gillies Hill rhyolite are differentially tilted across the Mineral Mountains as well (Fig. 1). Furthermore, paleomagnetic data show that magnetizations recorded by the dikes and the wall rocks are also perpendicular to each other between the two areas (*20*). Therefore, we interpret the difference in the orientation of planar markers to be the result of tilt that occurred after intrusion of the dikes.

On the eastern side of the Mineral Mountains, thrust faults, Paleozoic to Oligocene strata, and dikes are interpreted to be tilted 90° relative to correlative features on the northern and western sides of the batholith, whereas the 9-million-year-old Gillies Hill rhyolite is only tilted 30°. This observation suggests that the wall rocks and dikes were, in part, tilted before eruption of the rhyolite. Although the Gillies Hill rhyolite and the rhyolite dikes were interpreted to be correlative on the basis of petrography and K-Ar ages (*12*), we obtained a U-Pb zircon age for a rhyolite porphyry dike of 11.0 Ma (Fig. 2 and Table 1) (*21, 22*) and interpret this as the age of intrusion of the swarm (*23*). This age indicates that the dikes are not correlative with the Gillies Hill rhyolite, and therefore could have experienced tilting before extrusion of the rhyolite.

Given the listric geometry of the Beaver Valley fault and the evidence that Beaver Valley was open, in part, before eruption of the Gillies Hill rhyolite, a reasonable interpretation of the data is that deformation associated with the Beaver Valley fault is responsible for tilt of the rocks before 9 Ma. In this model (Fig. 3), at 11 Ma, subvertical rhyolite porphyry and diabase dikes intruded flat-lying Paleozoic and Oligocene strata. Between 11 and 9 Ma, Beaver Valley opened yielding up to 45° tilt of rocks on the eastern side of the batholith as a result of formation of a roll-over anticline above the Beaver Valley fault. The maximum amount of tilt of any hanging wall feature that can be accomplished as a result of this deformation is limited by the cutoff angle between it and the fault. Seismic imaging across Beaver Valley (6) suggests that, because of the listric geometry of the fault, this maximum should be approximately 60° on the eastern side of the Mineral Mountains and should rapidly decrease to 0° toward the west.

The Gillies Hill rhyolite erupted into Beaver Valley at 9 Ma, and subsequently or synchronously the batholith was unroofed along the Cave Canyon detachment fault (Fig. 3). Fission-track ages of 8 to 9 Ma for rocks on the western side of the Mineral Mountains suggest that cooling associated with unroofing occurred by 8 Ma (*24*). The Cave Canyon detachment fault and the Gillies Hill rhyolite experienced at least 30° tilt (*15*) after 9 Ma. Isolated mylonitic and cataclastic shear zones in the southeast part of the batholith dip moderately (20°) to the east (*7*); such an orientation suggests that up to 50° of tilt may have occurred locally, and dikes and wall rocks on the eastern side of the batholith presumably were tilted comparable amounts. We interpret this tilt to be the result of subvertical simple shear during isostatic rebound of the footwall because this mechanism will tilt all nonvertical markers. Thus, dikes on the eastern side of the batholith, which were tilted by motion on the Beaver Valley fault, are taken to subhorizontal dips whereas subvertical dikes away from the Beaver Valley breakaway, such as those on the western and northern sides of the batholith, remain subvertical. Simple shear may be recorded by numerous cataclastic zones and the overall microfractured texture of the batholith (*7, 10, 11*). This interpretation of the relative timing of motion of the Beaver Valley fault and Cave Canyon detachment fault predicts that the Beaver Valley fault should be deformed by footwall uplift as well. Available seismic data show a prominent domed reflector under the Mineral Mountains that may be continuous with the Beaver Valley fault [reflector A, figure 12 of (6)].

In contrast to evidence that some extensional core complexes developed without appreciable tilting of footwall rocks and the overlying fault, data from the Mineral Mountains indicate that core complexes and low-angle mylonitic detachment faults can develop as a result of tilting of initially moderately dipping faults. The Mineral Mountains lie at the southern end of one of the best known low-angle normal faults in the Basin and Range province, the Sevier Desert detachment. Thus, the nature of Basin and Range extensional deformation may change over short distances along strike. Finally, our data contradict models in which ductile deformation and rapid cooling is the result of shallow-level plutonism because there is no evidence for plutonic rocks associated with the Gillies Hill rhyolite in the vicinity of the exposed mylonitic detachment fault, and the bulk Mineral Mountains batholith intruded at least 7 million years before development of significant extensional faults.

REFERENCES AND NOTES

1. P. J. Coney, *Geol. Soc. Am. Mem.* **153**, 7 (1980).
2. B. P. Wernicke and G. J. Axen, *Geology* **19**, 848 (1988); R. W. Buck, *Tectonics* **7**, 959 (1988).
3. G. A. Davis and G. S. Lister, *Geol. Soc. Am. Spec. Pap.* **218**, 133 (1988); S. J. Reynolds and G. S. Lister, *Geology* **18**, 216 (1990); R. J. Scott and G. S. Lister, *ibid.* 20, 833 (1992); R. F. Livaccari, J. W.

Geissman, S. J. Reynolds, *Nature* **361**, 56 (1993).
4. G. S. Lister and S. L. Baldwin, *Geology* **21**, 607 (1993); T. Parsons and G. A. Thompson, *ibid.*, p. 247.
5. R. W. Allmendinger *et al.*, *ibid.* **11**, 532 (1983); D. B. von Tish, R. W. Allmendinger, J. W. Sharp, *Am. Assoc. Pet. Geol. Bull.* **69**, 1077 (1985).
6. R. B. Smith and R. L. Bruhn, *J. Geophys. Res.* **89**, 5733 (1984).
7. D. S. Coleman, thesis, University of Kansas (1991).
8. J. D. Walker and J. M. Bartley, in preparation.
9. M. N. Machette and T. A. Steven, *U.S. Geol. Surv. Mis. Invest. Map I-1455* (1983).
10. D. L. Nielson *et al.*, *Geology of Roosevelt Hot Springs KGRA, Beaver County, Utah* (Earth Science Laboratory, University of Utah Research Institute, Salt Lake City, 1978).
11. B. S. Sibbett and D. L. Nielson, *Geology of the Central Mineral Mountains, Beaver County, Utah* (Earth Sciences Laboratory Rep. 33, Utah University Research Institute, Salt Lake City, 1980).
12. D. L. Nielson, S. H. Evans, B. S. Sibbett, *Geol. Soc. Am. Bull.* **97**, 765 (1986).
13. J. N. Aleinikoff, D. L. Nielson, C. E. Hedge, S. H. Evans, *U.S. Geol. Surv. Bull. 1622* (1987).
14. D. S. Coleman and J. D. Walker, *J. Geophys. Res.* **92**, 11011 (1992).
15. D. E. Price and J. M. Bartley, *Geol. Soc. Am. Rocky Mtn. Sect. Abstr. Progr.* **24**, 58 (1992).
16. D. E. Price and J. M. Bartley, *Geol. Soc. Am. Cord. Sect. Abstr. Progr.* **22**, 76 (1990).
17. H. C. Liese, thesis, University of Utah (1957).
18. T. A. Steven, C. G. Cunningham, C. W. Naeser, H. H. Menhert, *U.S. Geol. Surv. Bull.* **1469** (1979).
19. S. H. Evans, T. A. Stevens, *Geol. Soc. Am. Bull.* **93**, 1131 (1982).
20. D. S. Coleman, J. W. Geissman, J. D. Walker, *Eos* **72**, 468 (1991). D. S. Coleman and J. W. Geissman, in preparation.
21. All samples were hand-picked to remove impurities, air-abraded, loaded into dissolution vessels, spiked with a mixed $^{205}Pb:^{235}U:^{233}U$ spike and dissolved in an $HF\text{-}HNO_3$ mixture at 220°C (*22*). Separation of U and Pb was accomplished using standard HCl chemistry. Pb and U were loaded on single Re filaments; Pb in silica gel plus H_3PO_4, and U in carbon plus H_3PO_4. All analyses were performed on the VG Sector 54 thermal ionization mass spectrometer housed at MIT. Lead was analyzed either in single-collector ion-counting mode, or static multicollector mode with ^{204}Pb measured using ion-counting. Uranium was measured as a metal ion in static multicollector mode.
22. R. R. Parrish, *Chem. Geol.* **66**, 99 (1987).
23. Reported K-Ar ages for the rhyolite porphyry dikes (*12*) agree well with those for the Gillies Hill rhyolite (*19*). However, K-Ar dates for intrusive rocks from the Mineral Mountains are consistently younger than U-Pb dates for the same phases (*7, 13*), and therefore probably represent cooling ages. We accept the K-Ar age for the Gillies Hill rhyolite as a crystallization age because it was obtained from an extrusive rock.
24. S. H. Evans and D. L. Nielson, *Geotherm. Res. Council Trans.* **6**, 15 (1982).
25. Supported by National Science Foundation grant EAR-8904007 to J.D.W. and Geological Society of America and Sigma Xi grants to D.S.C. We thank J. Bartley, J. Geissman, J. D. R. Applegate, S. Bowring, J. Fletcher, and B. Wernicke for helpful discussions, S. Coleman for mapping and sample collection, K. Davidek for sample preparation, and two anonymous reviewers.

30 July 1993; accepted 24 November 1993

Turbulent Mixing Under Drifting Pack Ice in the Weddell Sea

Miles G. McPhee and Douglas G. Martinson

By providing cold, dense water that sinks and mixes to fill the abyssal world ocean, high-latitude air-sea-ice interaction is the main conduit through which the deep ocean communicates with the rest of the climate system. A key element in modeling and predicting oceanic impact on climate is understanding the processes that control the near surface exchange of heat, salt, and momentum. In 1992, the United States–Russian Ice Station Weddell-1 traversed the western Weddell Sea during the onset of winter, providing a platform for direct measurement of turbulent heat flux and Reynolds stress in the upper ocean. Data from a storm early in the drift indicated (i) well-formed Ekman spirals (in both velocity and turbulent stress); (ii) high correlation between mixed layer heat flux and temperature gradients; (iii) that eddy viscosity and eddy thermal diffusivity were similar, about 0.02 square meters per second; and (iv) that the significant turbulent length scale (2 to 3 meters through most of the boundary layer) was proportional to the wavelength at the peak in the weighted vertical velocity spectrum. The measurements were consistent with a simple model in which the bulk eddy viscosity in the neutrally buoyant mixed layer is proportional to kinematic boundary stress divided by the Coriolis parameter.

Despite widespread interest in understanding how turbulence from wind stress and energy exchange at the surface distributes momentum, heat, and salt in the upper part of the ocean (*1*), direct flux measurements in the oceanic boundary layer (OBL) are rare, mostly because of the difficulty of measuring small turbulent fluctuations and mean flow gradients in the presence of a vigorous surface wave field. A largely unmet goal of oceanic turbulence research is the relation of the turbulent flux of a quantity to its mean gradient by means of an eddy diffusivity (or eddy viscosity if the quantity is vector momentum) coefficient. Eddy diffusivity, which depends more on the characteristics of the turbulent flow than on the particular fluid, is presumed to play a role in distributing properties analogous to that of molecular diffusivity but is generally much larger in geophysical flows. The concept has obvious utility for the modeling of the response of the upper ocean to changes in wind stress or surface fluxes of heat and salt.

Drifting sea ice effectively damps most surface waves and provides a stable platform from which it is relatively easy to deploy instruments sensitive enough to measure turbulence. In 1992, we maintained such equipment at several levels under the United States–Russian Ice Station Weddell-1 (ISW-1) as it drifted north in a region of multiyear pack ice east of the Antarctic Peninsula (*2*). In this report, we combine our direct measurements of turbulent heat flux and Reynolds stress (*3*) with basic planetary boundary layer theory and temperature-gradient data to estimate eddy viscosity and eddy thermal diffusivity. We also investigate the dominant length scale in the turbulent transfer process and describe a method for the estimation of its magnitude in the oceanic mixed layer.

By dimensional reasoning, eddy diffusivity, K, is the product of a turbulent velocity scale, u_*, and a turbulent length scale, λ. Within the lowest 20 or 30 m of the neutrally stable, atmospheric boundary layer (usually called the surface layer, as opposed to the outer or Ekman layer where rotation is important in the dynamics), numerous observations of velocity gradient (wind shear) and Reynolds stress have established that $u_* = u_{*0} = \sqrt{\tau_0}$ and $\lambda = \kappa z$, where τ_0 is the magnitude of kinematic boundary stress, z is height above the surface, and κ is von Kármán's constant (*4*). The results for the atmospheric surface layer cannot be extrapolated directly to the ocean because there is a large disparity in scales between the two boundary layers. A common assumption is that both extend to some proportion of the planetary scale, $u_{*0}/|f_{cor}|$, where f_{cor} is the Coriolis parameter (*5*), which implies that the governing scales differ roughly by the square root of the density ratio (a factor of about 30). The surface layer in the ocean is thus confined to the upper few meters. The neutrally buoyant outer layer typically extends to 1 to 2 km in the atmosphere and 30 to 60 m in the ocean. Although $\lambda = \kappa|z|$ formulations have been proposed for modeling of the oceanic boundary layer (*6*), numerical boundary layer models based on second-order turbulence closure (*7*) suggest that beyond the first few meters from the ocean surface (that is, beyond the surface layer), the mixing length is no longer proportional to z. Oceanic measurements and theoretical models typically focus on the outer OBL, where there is no widely accepted parameterization of λ and K.

M. G. McPhee, McPhee Research Company, 450 Clover Springs Road, Naches, WA 98937.
D. G. Martinson, Lamont-Doherty Earth Observatory and Department of Geological Sciences, Columbia University, Palisades, NY 10964.